조합하중을 받는 일정체적 캔틸레버 기둥의 정확탄성곡선

Elastica of Cantilever Column with Constant Volume Subjected to Combined Loads

이 병 구† 李 光 范* 윤 희 민**
Lee, Byoung-Koo Guangfan-Li Yoon, Hee-Min
(논문접수일 : 2007년 4월 20일 ; 심사종료일 : 2007년 5월 7일)

요 지

이 논문은 일정체적 캔틸레버 기둥의 정확탄성곡선(elastica)에 관한 연구이다. 기둥의 자유단에 압축하중과 모멘트 하중으로 구성되는 조합하중이 작용하는 캔틸레버 기둥의 정확탄성곡선을 지배하는 비선형 미분방정식과 경계조건을 유도하였다. 미분방정식에는 전단변형효과를 고려하였다. 기둥의 변단면으로는 정다각형 단면을 갖는 선형, 포물선형 및 정헌의 변단면을 채택하였다. 기둥의 정확탄성곡선을 해석하기 위하여 유도된 미분방정식을 수치해석하였다. 수치해석의 결과를 이용하여 기둥의 무차원 변수들이 정확탄성곡선에 미치는 영향을 분석하였다. 실험실 규모의 실험을 실시하여 이 연구에서 얻어진 수치해석의 결과를 검증하였다.

핵심용어 : 캔틸레버 기둥, 일정체적, 정확탄성곡선, 기하학적 비선형 해석, 조합하중, 실험

Abstract

This paper deals with the elastica of deflected cantilever column with the constant volume. The columns are subjected to combined loads consisted of an axial compressive load and a couple moment at the free end. Differential equations governing the elastica of such column are derived, in which both the effects of taper type and shear deformation are included. Three kinds of taper types are considered: linear, parabolic and sinusoidal tapers. Differential equations are solved numerically to obtain the elastica of objective columns. The effects of various system parameters on the elastica are investigated extensively. Experimental studies were carried out in order to verify the theoretical results of non-linear behavior of the elasticas.

Keywords : *cantilever column, constant volume, elastica, geometrical non-liner analysis, combined load, experiment*

1. Introduction

Since columns are basic structural forms, these units are widely used in structural engineering. In column problems, predicting both the buckling loads and post-buckling behavior are very important for column safety. Column responses under loadings depend on the cross-sectional shape, taper type, shear deformation, etc.(Haftka *et al*, 1990; Gere and Timoshenko, 1997)

The first studies of the large deformed shapes, namely elasticas, based on the elastica theory were published by Euler(1774). During the past few decades, elastica problems including column elasticas were discussed by many researchers. The works related to the present study, especially those involving the taper effect, shear deformation effect and experimental studies, were carried out by several

† Corresponding author and member · Department of Civil Engineering, Wonkwang University
Tel: 063-850-6718 ; Fax: 063-857-7204
E-mail: bkleest@wku.ac.kr
* Professor, Department of Civil Engineering, Hainan University
** Member and graduate student, Wonkwang University

• 이 논문에 대한 토론을 2007년 12월 31일까지 본 학회에 보내주시면 2008년 2월호에 그 결과를 게재하겠습니다.

researchers, e.g. those for the taper effect by Lee and Wilson(1993), Lee and Oh(2000) and Lee *et al.* (2002); those for the shear deformation effect by Huddleston(1972), Theocaris and Panayotounakos (1982), Sheinman and Adam(1987), Goto *et al.* (1990), and Sotiropoulou and Panayotounakos (2004); and those for experimental methods by Wilson *et al.*(1971), Lee and Wilson(1993), Lee *et al.*(2006) and Lee *et al.*(2007).

It is ideal that axial loads of columns are subjected exactly to the centroid of cross-section. However, all most of axial loads are acted on eccentrically so that it is desirable that the column loads are considered as the combined load consisted with both axial load and couple moment. In this work, the combined load is considered in the analysis of column behavior. Also, it is well known that the inclusion of shear deformation can increase the member deflections. For structural safety, it is necessary to include the shear deformation in structural analysis. Recently new structural materials have been developed and increasingly used in the structural work, which can sustain relatively large deflections compared with traditional materials. In these regards, the elastica problems of column including the buckling load, equilibrium path and stress resultant are very important in the analysis of column behavior. From all of these view points, this paper aims to analysis the geometrical non-linear responses of cantilever column subjected to combined loading. Herein, objective columns have the constant volume with the regular polygon cross-section. Such columns have to become tapers whose cross-sectional depth of column are varied along the column axis. In this study, three kinds of taper types are considered: linear taper, parabolic taper and sinusoidal taper. In the first author's pervious work(Lee *et al.* 2007), only the axial loads acted in centroid of the cross-section, i.e. not combined loading, have been analyzed.

In this paper, following assumptions are inherent: (1) column material is linear elastic; (2) column axis is incompressible; and (3) column is initially perfect. Under these assumptions, non-linear differential equations governing the elastica, i.e. deflected shape of column, are derived, in which the effect of shear deformation is included.

For solving differential equations, both Runge-Kutta and Regula-Falsi methods are used for integrating differential equations and for determining the unknown horizontal deflection of the free end, respectively. Through parametric studies, effects of taper type, section ratio and side number on the non-linear behavior such as equilibrium path, deflection, rotation, stress resultant and elastica are discussed in detail. Also, section ratios of the optimal column are determined from the parametric studies. Herein, an optimal column is defined as a column which has the minimum response under the given load condition. In addition, the theory and numerical methods of this study were validated by two sets of the laboratory scaled experiments.

2. Objective Columns

Shown in Fig. 1 is the configuration of an objective column with the length l whose volume V is always held constant. Its cross-sectional shape is the regular polygon with the integer side number $k \geq 3$. The cross-sectional depth is depicted as h which is varied along the axis s. Its area A and moment of inertia of area I are also varied with s. At the clamped end($s=0$), the depth is h_c, namely $h=h_c$, and at the free end($s=l$), $h=h_f$. For defining the column geometry, the section ratio a is introduced as

$$a = h_f / h_c \tag{1}$$

The values of A and I of the regular polygon cross-section with k and h are

$$A = a_1 h^2 \tag{2}$$

$$I = a_2 h^4 \tag{3}$$

where

$$a_1 = k\sin(\pi/k)\cos(\pi/k) \quad (4)$$

$$a_2 = (k/12)\sin(\pi/k)\cos^3(\pi/k)[3+\tan^2(\pi/k)] \quad (5)$$

The cross-section with $k=\infty$ is circular and its a_1 and a_2 are π and $\pi/4$, respectively. It is noted that every axis through the centroid of the regular polygon cross-section is a principal axis so that every monet of inertia of area I with respect to every principal axis is same.

The depth h which is a function of s is defined. Herein, three kinds of the functional variation h are chosen as: (1) linear; (2) parabolic; and (3) sinusoidal tapers. Since the functional equation h passes two points of $(0, h_c)$, $(l, \alpha h_c)$ in the co-ordinates(s, h) as shown in Fig. 1, each functional equation h can be determined as

• Linear taper

$$h = h_c[a_3(s/l)+1] \quad (6)$$

• Parabolic taper

$$h = h_c[a_3(s/l)^2+1] \quad (7)$$

• Sinusoidal taper

$$h = h_c[a_3\sin(\pi s/2l)+1] \quad (8)$$

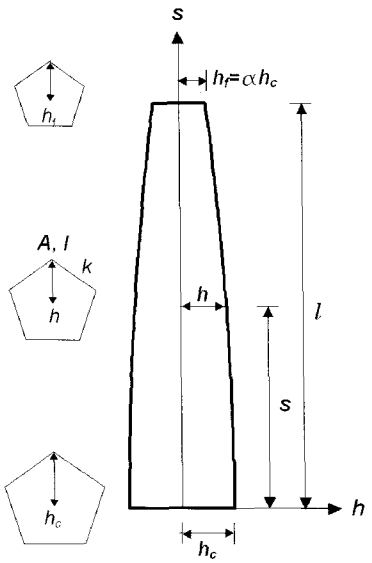

Fig. 1 Column with constant volume and regular polygon cross-section

where

$$a_3 = \alpha - 1 \quad (9)$$

The column volume V can be computed by using Eqs. (2) and (6)~(8), or

$$V = \int_0^l A ds = a_1 a_4 h_c^2 l \quad (10)$$

where

• Linear taper

$$a_4 = (\alpha^2+\alpha+1)/3 \quad (11)$$

• Parabolic taper

$$a_4 = (3\alpha^2+4\alpha+8)/15 \quad (12)$$

• Sinusoidal taper

$$a_4 = (\alpha-1)^2/2+4(\alpha-1)/\pi+1 \quad (13)$$

3. Governing Equations

3.1 Definition of Variables

Shown in Fig. 2(a) is a cantilever column placed on rectangular co-ordinates (x, y) whose origins

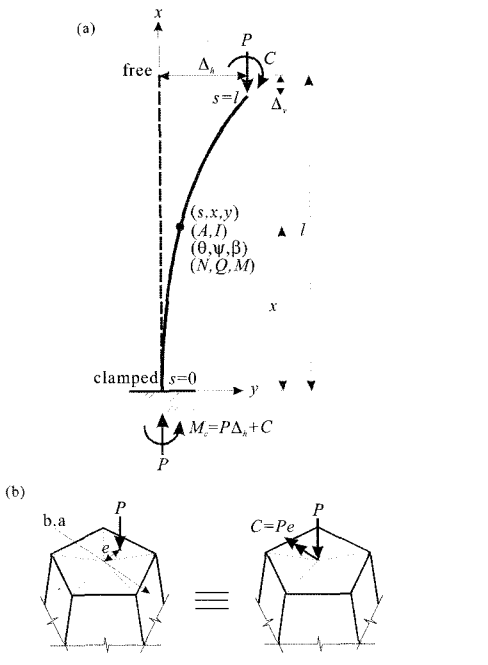

Fig. 2 (a) Column subjected to combined load; (b) relationships between P, C and e

are the clamped end. The dashed line represents the straight axis of column before loading. Meanwhile, the solid line depicts the deflected shape, namely elastica, after loading. The arc length measured from the clamped end to co-ordinates (x, y) is depicted as s. At the free end, the centroidal load P and couple moment C are carried out combinedly. These loads are equivalent to an axial load P with the eccentric distance $e = C/P$. Therefore, P with $C = 0$ represents one centroidal load, and C with $P = 0$ represents the pure bending.

The relationship between P, C and e is illustrated in Fig. 2(b). Since every axis passing the centroid is a principal axis of cross-section, the vertical axis to the line linked with the centroid and acting point of the load becomes the bending axis(b.a).

Before loading, both s-and x-axes are coincide. However, s-axis is departed from x-axis and two axes are no more coincide when the column is deformed by loads. Because of incompressibility of the column axis, the length of deflected column sustains its original length l. Therefore, value s of elastica at the free end is l. The deflected column is subjected to the stress resultants: normal force N, shear force Q, and bending moment M. Column rotation θ consists of rotation ϕ due to M and rotation β due to Q. At the free end($s = l$), the horizontal and vertical deflections and rotation are depicted as Δ_h, Δ_v and θ_f, respectively. At the clamped end($s = 0$), both the vertical reaction P and reaction moment $M_c = P\Delta_h + C$ are subjected. At the free end of elastica, the deflection Δ_h is unknown so that $M_c(= P\Delta_h + C)$ at the clamped end becomes an undeterminant and subsequently, co-ordinates (x, y), rotations (ϕ, β) and stress resultants (N, Q, M) are also unknown. Once again, it is accentuated that the determining all of these unknowns including (x, y), (ϕ, β) and (N, Q, M) of the elastica is the essential point of this study.

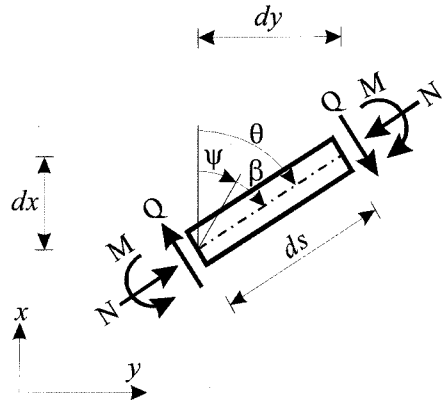

Fig. 3 Positive stress resultant and rotation

3.2 Derivation of Differential Equations

Shown in Fig. 3 are the positive sign convention of stress resultant and rotation of cross-section. Referring the sign convention and also applying equilibrium equations in Fig. 2, stress resultants N, Q and M at any co-ordinates (x, y) are obtained. The results are

$$N = P\cos\theta \tag{14}$$

$$Q = P\sin\theta \tag{15}$$

$$M = P\Delta_h + C - Py \tag{16}$$

As shown in Fig. 3, the total rotation θ consists of ϕ due to M and β due to Q. It is natural that the following equation is obtained.

$$\theta = \phi + \beta \tag{17}$$

Stress resultants M and Q can be expressed by the rotations ϕ and β, respectively. The results are

$$M = EI\frac{d\phi}{ds} \tag{18}$$

$$Q = fGA\beta \tag{19}$$

Here, E is Young's modulus, G is shear modulus of elasticity and f is shape factor. Value of f is: $f = 0.417$ for $k = 3$, $f = 0.833$ for $k = 4$ and $f = 0.900$ for $k \geq 5$(Arbabi, 1991).

Following equation is obtained by differentiating Eq. (17) with respect s.

$$\frac{d\theta}{ds} = \frac{d\psi}{ds} + \frac{d\beta}{ds} \tag{20}$$

First order derivatives of $d\psi/ds$ and $d\beta/ds$ in Eq. (20) are now determined. Substituting Eq. (16) to Eq. (18) and rearranging about the term of $d\psi/ds$ give $d\psi/ds$, and $d\beta/ds$ is obtained by differentiating Eq. (19) with respect to s. Two results are

$$\frac{d\psi}{ds} = \frac{1}{EI}(P\Delta_h + C - Py) \tag{21}$$

$$\frac{d\beta}{ds} = -\frac{1}{fGA}\left(\frac{dQ}{ds} - \frac{Q}{A}\frac{dA}{ds}\right) \tag{22}$$

Both derivatives dQ/ds and dA/ds in Eq. (22) are obtained. Derivative dQ/ds is obtained by differentiating Eq. (15) with respect to s.

$$\frac{dQ}{ds} = P\cos\theta\frac{d\theta}{ds} \tag{23}$$

By using Eqs. (2) and (6)~(8), first order derivative dA/ds by taper type is obtained as follows.

• Linear taper

$$\frac{dA}{ds} = \frac{2a_1a_3h_c^2}{l}\left[a_3\left(\frac{s}{l}\right)+1\right] \tag{24}$$

• Parabolic taper

$$\frac{dA}{ds} = \frac{4a_1a_3h_c^2}{l}\left(\frac{s}{l}\right)\left[a_3\left(\frac{s}{l}\right)^2+1\right] \tag{25}$$

• Sinusoidal taper

$$\frac{dA}{ds} = \frac{a_1a_3\pi h_c^2}{l}\cos\left(\frac{\pi s}{2l}\right)\left[a_3\sin\left(\frac{\pi s}{2l}\right)+1\right] \tag{26}$$

Differential equations governing the elastica of deflected column can be derived. Substituting Eq. (3) to Eq. (21) gives the equation of $d\psi/ds$, and substituting Eqs. (2), (15) and (23)~(26) gives the equation of $d\beta/ds$. And then substituting two equations of $d\psi/ds$ and $d\beta/ds$ to Eq. (20) gives the non-linear differential equation as

$$\frac{d\theta}{ds} = \frac{1}{1-\dfrac{P\cos\theta}{fGa_1h_c^2H_1^2}}\left[\frac{P\Delta_h + C - Py}{Ea_2h_c^4H_1^4} - \frac{Pa_3\sin\theta H_2}{fGa_1h_c^2H_1^3}\right],\quad 0\le s\le l \tag{27}$$

where H_1 and H_2 are

• Linear taper

$$H_1 = a_3(s/l)+1 \tag{28}$$

$$H_2 = 2/l \tag{29}$$

• Parabolic taper

$$H_1 = a_3(s/l)^2+1 \tag{30}$$

$$H_2 = 4s/l^2 \tag{31}$$

• Sinusoidal taper

$$H_1 = a_3\sin(\pi s/2l)+1 \tag{32}$$

$$H_2 = (\pi/l)\cos(\pi s/2l) \tag{33}$$

Referring Fig. 3 depicting the trigonometric relationship, well-known differential equations are obtained, or

$$\frac{dx}{ds} = \cos\theta,\quad 0\le s\le l \tag{34}$$

$$\frac{dy}{ds} = \sin\theta,\quad 0\le s\le l \tag{35}$$

Equations (27), (34) and (35) are differential equations governing the elastica of deflected column with the constant volume. These equations are typical geometrical non-linear differential equations so that the non-linear behavior of column such as equilibrium path can be analyzed.

Since the rotation and deflections are not allowed at the clamped end($s=0$), boundary conditions are obtained as

$$\theta_{s=0} = 0 \tag{36}$$

$$x_{s=0} = 0 \tag{37}$$

$$y_{s=0} = 0 \tag{38}$$

It is fact that differential Eqs. (27), (34) and (35) subjected to the boundary conditions of Eqs. (36)~(38) are fittable on the initial value problem. Since Eq. (27) contains the unknown Δ_h, this

equation can not be integrated even though all boundary conditions at $s=0$ are already known as shown in Eqs. (36)~(38). The horizontal deflection of the free end($s=l$) is Δ_h, i.e. $y_{s=l}=\Delta_h$, and therefore, the boundary condition at the free end is obtained as follows.

$$y_{s=l}-\Delta_h=0 \tag{39}$$

3.3 Non-dimensional Governing Equations

To facilitate the numerical studies and to obtain the most general results for this class of problem, the following non-dimensional system parameters are defined. Parameters related to the co-ordinates are introduced as

$$\lambda=s/l \tag{40}$$
$$\xi=x/l \tag{41}$$
$$\eta=y/l \tag{42}$$
$$\delta_h=\Delta_h/l \tag{43}$$
$$\delta_v=\Delta_v/l \tag{44}$$

where (λ, ξ, η) are non-dimensional co-ordinates normalized by the length l and (δ_h, δ_v) are non-dimensional deflections at the free end($\lambda=1$).

Shear parameter g which is related to the material properties and aspect ration r which is related to l and V are defined, respectively, as

$$g=G/E \tag{45}$$
$$r=(l^3/V)^{1/2} \tag{46}$$

Finally, loads P and C are normalized as follows.

$$p=Pl^4/(EV^2) \tag{47}$$
$$c=Cl^3/(EV^2) \tag{48}$$

For converting dimensional Eqs. (27), (34) and (35) to non-dimensional ones, the terms of dy/ds, $dx/ds$and dy/ds are rewritten as follows.

$$\frac{d\theta}{ds}=\frac{d\theta}{d(l\lambda)})=\frac{1}{l}\frac{d\theta}{d\lambda} \tag{49}$$
$$\frac{dx}{ds}=\frac{d(l\xi)}{d(l\lambda)}=\frac{d\xi}{d\lambda} \tag{50}$$
$$\frac{dy}{ds}=\frac{d(l\eta)}{d(l\lambda)}=\frac{d\eta}{d\lambda} \tag{51}$$

Using all equations mentioned above, non-dimensional differential equations are obtained. Substituting the derivative terms of Eqs. (49)~(51) to differential Eqs. (27), (34) and (35), and using parameters in Eqs. (40)~(48) give the non-linear differential equation. The result is

$$\frac{d\theta}{d\lambda}=\frac{p}{\frac{i_1^3}{a_4}-\frac{pi_1\cos\theta}{fgr^2}}\left[\frac{a_1^2a_4(\delta_h+c/p-\eta)}{a_2i_1}-\frac{i_2\sin\theta}{fgr^2}\right],\ 0\le\lambda\le1 \tag{52}$$

where i_1 and i_2 are

• Linear taper

$$i_1=a_3\lambda+1 \tag{53}$$
$$i_2=2a_3 \tag{54}$$

• Parabolic taper

$$i_1=a_3\lambda^2+1 \tag{55}$$
$$i_2=4a_3\lambda \tag{56}$$

• Sinusoidal taper

$$i_1=a_3\sin(\pi\lambda/2)+1 \tag{57}$$
$$i_2=(a_3\pi)\cos(\pi\lambda/2) \tag{58}$$

Also dimensional Eqs. (34) and (35) are transformed into non-dimensional ones easily. The results are

$$\frac{d\xi}{d\lambda}=\cos\theta,\ 0\le\lambda\le1 \tag{59}$$
$$\frac{d\eta}{d\lambda}=\sin\theta,\ 0\le\lambda\le1 \tag{60}$$

The boundary conditions of Eqs. (36)~(39) can be converted to the non-dimensional ones by using Eqs. (40)~(43) as follows.

$$\theta_{\lambda=0}=0 \tag{61}$$

$$\xi_{\lambda=0}=0 \tag{62}$$

$$\eta_{\lambda=0}=0 \tag{63}$$

$$\eta_{\lambda=1}-\delta_h=0 \tag{64}$$

Finally, stress resultants N, Q and M are normalized as follows.

$$n=Nl^4/(EV^2)=p\cos\theta \tag{65}$$

$$q=Ql^4/(EV^2)=p\sin\theta \tag{66}$$

$$m=Ml^3/(EV^2)=p\delta_h+c-p\eta \tag{67}$$

4. Numerical Examples and Discussion

4.1 Convergence Analysis

When appropriate numerical methods are applied into differential Eqs. (52), (59) and (60), the elastica of (ξ, η) and stress resultants of (n, q, m) under a given load set of (p and c) accompanying with a given column geometry of (taper type, k, α, r and g). The Runge-Kutta method is used for integrating differential equations subjected to the boundary conditions and Regula-Falsi method is used for determining the unknown δ_h, respectively. In solving differential equations containing the unknown as the initial value problem, such numerical methods were already verified in many works(Lee *et al.*, 2005).

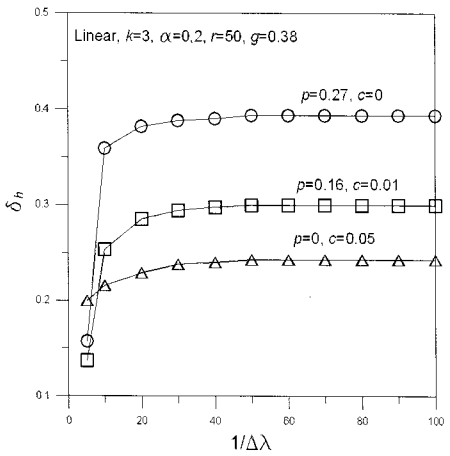

Fig. 4 Convergence analysis

Prior to executing numerical examples, convergence analyses were done for determining the suitable step size $\Delta\lambda$ in the Runge-Kutta method. Figure 4 shows results of convergence analysis about the horizontal deflection δ_h at the free end. Input variables used in the analysis are shown in

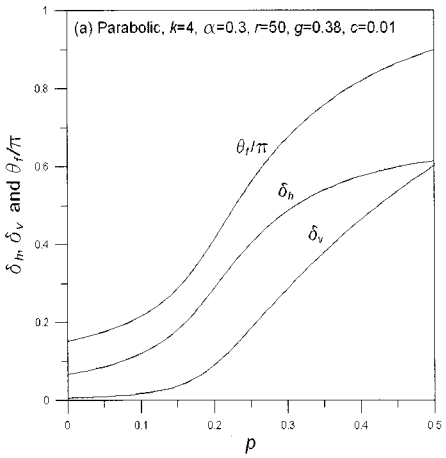

(a) combined load

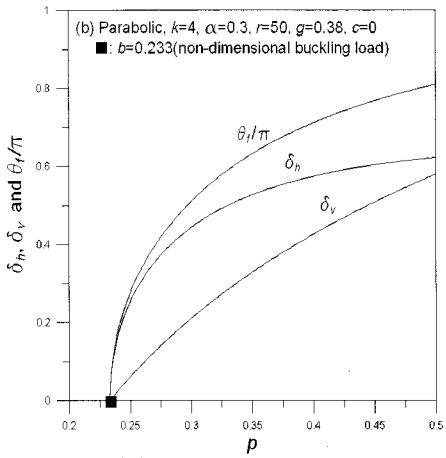

(b) centroidal load

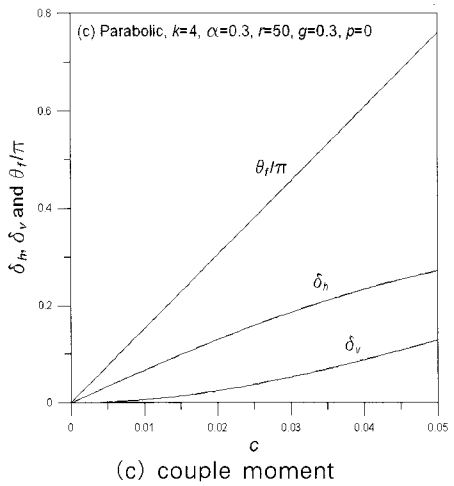

(c) couple moment

Fig. 5 Equilibrium paths

Fig. 4. It is seen that numerical solutions of δ_h with $1/\Delta\lambda = 40$, i.e. step size $\Delta\lambda = 1/40$, are sufficiently converged to those with $1/\Delta\lambda = 100$. In order to increase the accuracy of the numerical solutions, all solutions of this study are obtained under $1/\Delta\lambda = 50$ with which solutions have the three significant figures comparing those with $1/\Delta\lambda = 100$.

4.2 Equilibrium Paths

Shown in Fig. 5(a), (b) and (c) are the equilibrium paths which represent relationship between load and deflection. See the input variables of each column in each figure. Equilibrium paths are typically non-linear as expected. In Fig. 5(a), the column behavior has been already arisen even though p is zero because the column has been already subjected to the couple moment $c = 0.01$. In Fig. 5(b), the column is straight before column buckles under $p = 0.233$ marked ■ on the p-axis. Therefore, non-dimensional load $p = 0.233$ becomes the non-dimensional buckling load b defined as $b = Bl^4/(EV^2)$ where B is the buckling load. In Fig. 5(c) of the case of pure bending, i.e. $p = 0$, non-linearities are relatively smaller than those of Fig. 5(a) and 5(b).

4.3 Parametric Studies

Column behavior is seriously influenced by column parameters and it is important to analysis effects of column parameters on column behavior.

Table 1 shows the effect of taper type on responses of δ_h, δ_v and θ_f of the free end. Responses are smaller from parabolic to linear to sinusoidal tapers. Consequently, the parabolic taper is most robust against the column behavior among three tapers under other conditions are held constant. For an example, the ratio of sinusoidal taper to parabolic one for δ_h with the loads of $p = 0.2$ and $c = 0.01$ is $0.4445/0.2462 = 1.81$ so that the column of sinusoidal taper responds about 81% greater than that of parabolic one.

Effect of side number k on responses of δ_h, δ_v and θ_f is shown in Table 2. Responses are smaller from $k = 3$ to 4 to 5 to $k = \infty$ orderly. The regular triangular($k = 3$) cross-section is most robust among the regular polygon ones under other conditions are the same. For an example, the ratio of $k = \infty$ to $k = 3$ for δ_h with $p = 0.2$ and $c = 0.01$ is $0.3773/0.2175 = 1.73$. The column of circular cross-section($k = \infty$) responds 73% greater than that of triangular one($k = 3$). From results of Table 1 and 2, it is concluded that the parabolic tapered column with the regular triangular cross-section is the strongest column among columns combining with taper types and integer side number k.

Table 3 shows the effect of aspect ratio r on responses of δ_h, δ_v and θ_f. Greater r yields smaller response. The aspect ratio is decreasing effect on column behavior. However its decreasing rate is very small and then its effect is negligible. In addi-

Table 1 Effect of taper type on δ_h, δ_v and θ_f

Load	Res.	Linear	Parabolic	Sinusoidal
$p=0.2$ $c=0.01$	δ_h	0.3179	0.2462	0.4445
	δ_v	0.0980	0.0531	0.2506
	θ_f	1.0079	0.8017	1.5817
$p=0.3$ $c=0$	δ_h	0.5084	0.4638	0.5299
	δ_v	0.2835	0.1949	0.4330
	θ_f	1.5749	1.2988	2.0166

* $k=5, \alpha=0.4, r=50, g=0.38$; Res.: Responses

Table 2 Effect of k on δ_h, δ_v and θ_f

Load	Res.	$k=3$	$k=4$	$k=5$	$k=\infty$
$p=0.2$ $c=0.01$	δ_h	0.2175	0.3365	0.3626	0.3773
	δ_v	0.0422	0.1056	0.1246	0.1363
	θ_f	0.5871	0.9186	0.9976	1.046
$p=0.3$ $c=0$	δ_h	0.4350	0.5386	0.5520	0.5588
	δ_v	0.1838	0.3256	0.3520	0.3669
	θ_f	1.1515	1.5644	1.6329	1.6705

* Sinusoidal taper, $\alpha=0.5$, $r=50$, $g=0.38$

Table 3 Effect of r on δ_h, δ_v and θ_f

Load	Res.	$r=50$	$r=75$	$r=100$	$r=\infty$
$p=0.2$ $c=0.01$	δ_h	0.2641	0.2640	0.2640	0.2639
	δ_v	0.0533	0.0533	0.0533	0.0533
	θ_f	0.6044	0.6043	0.6042	0.6041
$p=0.3$ $c=0$	δ_h	0.5646	0.5645	0.5645	0.5644
	δ_v	0.2841	0.2840	0.2839	0.2839
	θ_f	1.3177	1.3174	1.3172	1.3171

* Linear taper, $k=\infty$, $\alpha=0.6$, $g=0.38$

tion, when r is neglected in the theory, the differential Eq. (52) is reduced to the simple equation of

$$\frac{d\theta}{d\lambda}=\frac{a_1^2a_4^2}{a_2i_1^4}(p\delta_h+c-p\eta) \tag{68}$$

Note that using above equation instead of Eq. (52) yields the responses slightly underestimated. Therefor, it is useful to use Eq. (68) in cases of highly slender columns.

4.4 Optimal Section Ratios

It is important to find out the optimal shape of column whose responses become minimum under the given load condition. Shown in Fig. 6(a) and 6(b) are the α versus(δ_h, δ_v and θ_f) curves. See input parameters in each figure. In Fig. 6(a), each response of δ_h, δ_v and θ_f decreases and reaches each minimal response and increases as section ratio α increases. In each curve of Fig. 6(a), each lowest point is marked as ○, whose response is minimized at the corresponding α value. For an example, minimal response of $\delta_h=0.130$ is arisen at $\alpha=0.549$. This means that optimal section ratio α is determined as $\alpha_{opt}=0.549$ against the minimal $\delta_h=0.130$ for a given load condition($p=0.2$ and $c=0.01$) and geometry of column(parabolic, $k=3$, $r=50$, $g=0.38$). Similarly, $\alpha_{opt}=0.584$ for minimal $\delta_v=0.0126$ and $\alpha_{opt}=0.682$ for minimal $\theta_f=$

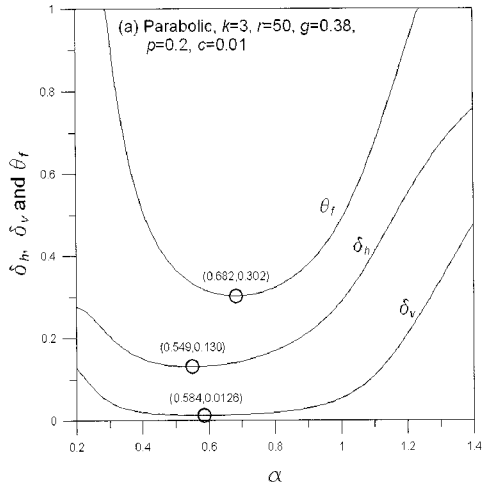

(a) combined load

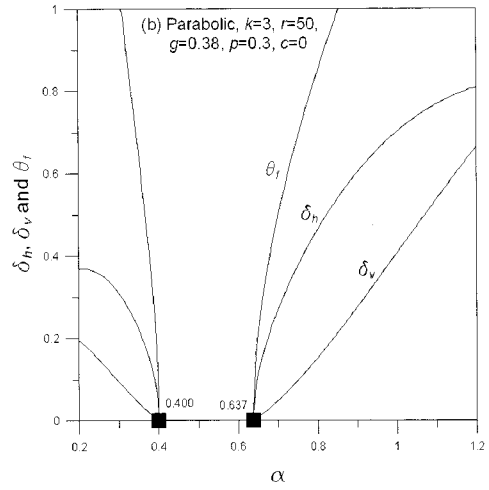

(b) centroidal load

Fig. 6 α versus (δ_h, δ_v and θ_f) curves

0.302 are obtained. As discussed in this example, optimal section ratios α_{opt} for a given column condition can be determined. Figure 6(b) shows the response variations of δ_h, δ_v and θ_f in case of the centroidal load($p=0.3$, $c=0$). Both minimum and maximum α values are marked as ■ on α-axis, at which the column does not buckle under the given condition(parabolic taper, $k=3$, $r=50$, $g=0.38$, $p=0.3$, $c=0$). The column is straight in the range of $0.400<\alpha<0.637$ and while in the range of $\alpha<0.400$ and $\alpha>0.637$, the column buckles. As shown in this example, the stable region of α in which the column does not buckle can be determined. These kinds of figures are useful for designing the optimal columns.

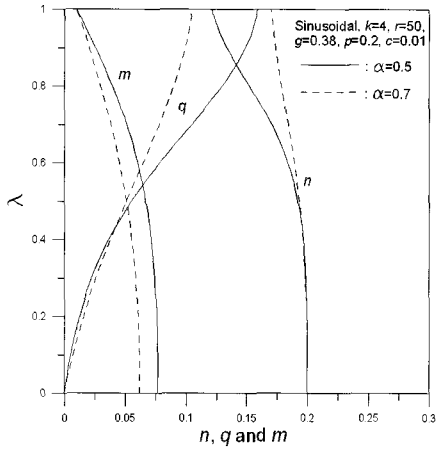

Fig. 7 Diagrams of stress resultants

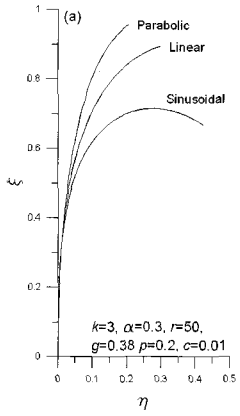

(a) taper type(linear, parabolic and sinusoidal)

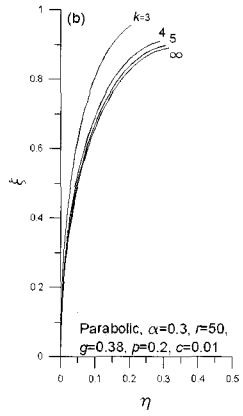

(b) side number k

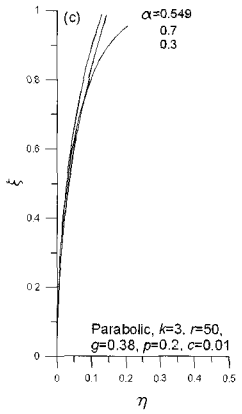

(c) section ratio α

Fig. 8 Elasticas

4.5 Stress Resultants and Elasticas

Fig. 7 shows diagrams of the stress resultants n, q and m loaded on the cross-section. See input variables of the columns in the figure. Stress resultants n and m are greatest at the clamped end while zero at the free end. Meanwhile, the reverse is fact for the stress resultant q.

Typical elasticas of deflected shape of column are shown in Fig. 8(a), (b) and (c). Load and geometry of column are shown in each figure. From these figures, it is clear that the parabolic taper with triangular($k=3$) cross-section and section ratio $\alpha_{opt}=0.549$ is the strongest column comparing other geometries for the given loads($p=0.2$ and $c=0.01$).

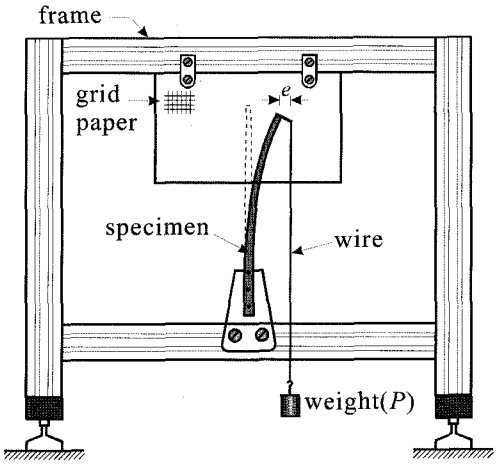

Fig. 9 Experimental set up

5. Experiments

5.1 Experimental Process

For validating the theory and numerical methods developed herein, two sets of laboratory scaled experiments were done. Shown in Fig. 9 is the schematic view of the experimental set up. Specimen column is fixed on the steel frame. At the free end, a rigid stub is sticked and the weight(P) is hanging at the tip for realizing the eccentric load. It is noted that the eccentric distance e is the vertical length measured from the centroid to the wire axis after final deforming state as shown in Fig. 9. This load system is equivalent to the combined load with P and $C=Pe$. For measuring the deflections, grid paper is attached on the backboard of the experimental frame.

Prior to executing experiments, the load which causes moderate deflections is pre-computed by the

theory. The weight is increased slowly to the pre-computed load P and then the equilibrium state is performed finally. By using the digital camera, photographs of deformed shapes are taken, enlarged photographs are printed out and those deflections and rotations are measured by the calipers and angle meter, respectively. Readers can refer the work by Wilson(1993) who discusses this kind of experiments in detail.

5.2 Geometry of Specimen Columns

According to the experimental process, two sets of experiments were done. Specimen columns were chosen as the linear taper with square cross-section ($k=4$) which may be relatively easy to make. Plastic was used for the column material whose properties are $E=3.4\times10^3$ N/mm^2 and $G=1.21\times10^3$ N/mm^2 and thus its non-dimensional system parameter $g=0.357$. Loads and geometries of the specimens in experiments are:

- Specimen A: Centroidal load
  $l=250$ mm, $h_c=8.7$ mm, $h_f=4.2$ mm and $P=45$ N for which its system parameters are $a=0.483$, $r=33.7$ and $p=0.256$

- Specimen B: Eccentric load
  $l=300$ mm, $h_c=9.6$ mm, $h_f=4.2$ mm, $P=31$ N and $e=14.5$ mm for which its system parameters are $a=0.438$, $r=40.5$, $p=0.248$, $e/l=0.0484$ and $c=0.0120(=0.248\times0.0484)$

Note that the specimen A is subjected to the centroidal load and the specimen B is subjected to the eccentric load, namely combined load with P and $C=Pe$.

5.3 Experimental Results

Deflections and rotations are measured from the enlarged photos, and normalized, and compared with those computed by the theory in Table 4 in which δ_h, δ_v and θ_f at $\lambda=1$(free end)), and the horizontal deflection η, vertical deflection $\lambda-\xi$ and rotation θ at $\lambda=2/3$ are reported. Table shows that average errors are about 3.54% in case of the specimen A and about 5.45% in case of the specimen B. Perhaps, defaults of manufacturing the specimen and also excluding the material non-linearity in the theory may yield such discrepancies. Considering that two results by theory and experiment are agreed quite well, the theory developed herein is validated.

6. Conclusions

This paper deals with the geometrical non-linear analysis of the cantilever column. Objective columns have the constant volume with the regular polygon cross-section whose depth is varied with the linear, parabolic and sinusoidal functional fashions. At the

Table 4 Comparisons of column responses between theory and experiment

• Specimen A: Centroidal load

Position	Res.	Theory	Experi.	Error(%)*
$\lambda=1$	δ_h	0.199	0.205	3.02
	δ_v	0.0318	0.0330	3.77
	θ_f	0.470	0.480	2.13
$\lambda=2/3$	η	0.0734	0.0712	3.00
	$\lambda-\xi$	0.00620	-	-
	θ	0.278	0.262	5.76

• Specimen B: Eccentric load

Position	Res.	Theory	Experi.	Error(%)*
$\lambda=1$	δ_h	0.443	0.462	4.29
	δ_v	0.195	0.182	6.67
	θ_f	1.341	1.392	3.80
$\lambda=2/3$	η	0.165	0.152	7.88
	$\lambda-\xi$	0.0333	0.0352	5.71
	θ	0.671	0.642	4.32

* Error(%) = |1 − Experiment / Theory| ×100

free end, the combined load consisted of an axial load and a couple moment. Following results are obtained:

1) Differential equations governing the elastica of column subjected to the combined loading are derived.

2) Columns are more robust against the responses from the parabolic to linear to sinusoidal tapers.

3) Columns with the smaller side number(k) yield the smaller responses.

4) Aspect ratio(r) is the decreasing effect on the column responses but this effect is negligible.

5) Optimal section ratios(α_{opt}) can be determined by reading the lowest points of the respective α versus responses curves.

6) Through the laboratory scaled experiments, the theories developed in this study are validated.

Acknowledgement

This work was supported by Wonkwang University in 2007. First author appreciates this financial support.

References

Arbabi, F. (1991) *Structural Analysis and Behavior*. McGraw-Hill, Inc.

Euler, L. (1774) Methodus inveniendi lineas curvas maxima minimive proprietate gaudentes, Additamentum I. *De Curvis Elasticis*, Lausanne and Geneva.

Gere, J.M., Timoshenko, S.P. (1997) *Mechanics of Materials*, PWS Publishing Company.

Haftka, R.T., Gurdal, Z., Kamat, M.P. (1990) *Element of Structural Optimization*, Kluwer Academic Publisher.

Lee, B.K., Carr, A.J., Lee, T.E., Ahn, D.S. (2005) Elasticas and buckling loads of shear deformable tapered columns. *International Journal of Structural Stability and Dynamics*, 5(3), pp.317~335.

Lee, B.K., Carr, A.J., Lee, T.E., Kim, I.J. (2006) Buckling loads of columns with constant volume. *Journal of Sound and Vibration*, 294, pp.381~387.

Lee, B.K., Kim, S.K., Lee, S.W. (2007) Geometrical non-linear analysis of cantilever column with constant volume, *Journal of Korean Society of Civil Engineers*, 27(1A), pp.59~67(in Korean).

Lee, B.K., Kim, S.K., Park, K.K. (2006) Critical loads of tapered Beck's columns with clamped and spring supports. *Journal of the Computational Structural Engineering Institute of Korea*, 19(1), pp.85~92(in Korean).

Lee, B.K., Oh, S.J. (2000) Elastica and buckling loads of simple tapered columns with constant volume. *International Journal of Solids and Structures*, 37, pp.2507~2518.

Sakiyama, T. (1986) A method of analyzing the elastic buckling of tapered columns. *Computers & Structures*, 23(1), pp.119~120.

Takagi R., Maeda M., S. J. Duan, S.J., Nakagawa, K. (1997) A proposal for optimum structural design with the largest buckling load. *Computer & Structures*, 63(5), pp.1033~1036.

Wilson, J.F. (1993) *Experiments of the Strength of Solids*, McGraw-Hill, Inc.

Wilson, J.F., Holloway, D.M. (1971) Stability experiments on the strongest columns and circular arches. *Experimental Mechanics*, 11, pp.303~308.